JOURNAL OF MATERIALS SCIENCE 33 (1998) 3823–3830

Oxidation behaviour of alumina–silicon carbide nanocomposites

D. SCITI
Enricerche, S. Donato Milanese, Italy
A. BELLOSI
CNR-IRTEC,Via Granarolo 64, Faenza, Italy
E-mail: bellosi@irtecl.irtec.bo.cnr.it

Oxidation studies were conducted on Al_2O_2–SiC nanocomposites at 1400 °C. The composites were prepared by hot-pressing mixtures of commercial alumina and ultrafine SiC powders, in amounts of 5, 15 and 30 vol %. Linear kinetics were detected for the oxidation of composites containing 5 vol % SiC. Two stages were observed in composites containing 15 vol % SiC: the first linear and the second presumably parabolic. A parabolic behaviour was observed in the sample containing 30 vol % SiC. The oxidation rates were several orders of magnitude higher than those of monolithic SiC and the observed data were not consistent with the expected increase in weight associated with the oxidation reaction of SiC to SiO_2; in fact the most surprising feature is that the sample containing 30 vol % SiC showed a better oxidation resistance than samples containing 5 and 15 vol % SiC. The reaction products were alumina and mullite in samples with 5 and 15 vol % SiC, while mullite and silica were found on the oxidized surface of samples containing 30 vol % SiC. Explanations are given of the influence of the oxidizable phase amount, the presence of impurities, reaction product structure and composition.

1. Introduction

Silicon carbide-containing nanocomposites are attracting growing interest, owing to the increasing emphasis on structural ceramics for high-temperature applications. Significant improvements in strength and toughness have been reported for Al_2O_3 containing fine SiC particles [1–3], even though the results in terms of microstructure and properties strictly depend on processing and on composition and grain size of the employed powders [1–20]. Research has been directed primarily towards an understanding of the mechanical properties at both room and elevated temperature, while little attention has been given to the environmental compatibility of this class of composites. Alumina, as a stable high-temperature oxide and potential good barrier against oxygen diffusion, is a viable candidate as a matrix material. Monolithic silicon carbide is known to have an excellent oxidation resistance, because it forms a protective film of silica [21]. However, the oxidation resistance of silicon carbide-containing composites is influenced by the matrix constituent, because of possible interactions between the silica and the matrix [21–24].

Studies on the silicon carbide–alumina composites indicate parabolic kinetics, with rate constants which increase with the volume fraction of micrometre-sized SiC particles and are higher by a factor of $\sim 10^3$ than those for oxidation of SiC [21, 25]. In another study [26], Al_2O_3–5 vol % SiC nanocomposites show very little oxidation, with oxide layers lower than $\sim 2\mu m$ even after 96 h at 1350 °C. The transport phenomena active during oxidation of alumina/silicon carbide systems are rather complex, involving aluminium-doped silica adjacent to the oxidizing SiC, mullite formation, and the interaction of the reaction products with the crystalline Al_2O_3 matrix.

The purpose of the present study was to ascertain the high-temperature (1400 °C) oxidation behaviour of Al_2O_3–SiC nanocomposites, containing 5, 15 and 30 vol % nanosized SiC particles, through the analysis of reaction products and kinetics.

2. Experimental procedure

Oxidation studies were conducted on the following hot-pressed nanocomposites: Al_2O_3 + 5 vol % SiC (sample A5), Al_2O_3 + 15 vol % SiC (sample A15), Al_2O_3 + 30 vol % SiC (sample A30).

Raw materials were α-Al_2O_3 (Ceralox HPA0.5, specific surface area 11 m^2g^{-1}, impurities sodium, iron, calcium and magnesium amounts from 10–30 p.p.m.) and β-SiC produced by laser-induced gas phase reaction (ENEA, Italy, s.s.a. 42 m^2g^{-1}). Details on the preparation of powder mixes, hot pressing, microstructure and mechanical properties of the samples are reported elsewhere [20].

Table I lists the main characteristics of the nanocomposites in comparison with the values of

TABLE I Hot-pressing (HP) conditions (applied pressure 30 MPa), final relative density, (ρ), mean grain size of alumina, d, Vickers hardness, HV1.0, fracture toughness, (K_{Ic}), Young's modulus, E, four-point flexural strength, σ, of the tested composites. For a comparison, the values relative to monolithic alumina (sample A) are also shown [20].

Sample	HP	ρ (%)	d (μm)	HV1.0 (GPa)	K_{Ic} (MPa $m^{1/2}$)	E (GPa)	σ (MPa)
	T(°C) t (min)						
A5	1700 15	98.8	0.34	20.4 ± 0.4	3.8 ± 0.2	357 ± 4	642 ± 102
A15	1750 20	97.6	0.30	20.1 ± 0.5	4.0 ± 0.2	346 ± 3	
A30	1800 35	99.8	0.29	22.5 ± 0.8	3.7 ± 0.2	346 ± 3	
A	1500 10	100	1.20	18.7 ± 0.6	3.2 ± 0.2	387 ± 4	430 ± 36

monolithic alumina. Despite the high hot-pressing temperatures, the final microstructures are very fine, as shown in Fig. 1a–c. SiC particles (40–60 nm) are located mainly at the grain boundaries, and to a lesser extent inside alumina grains. In addition, amorphous silicate–mullite like phases, arising from the reaction of the silica present in the SiC powder with alumina and its impurities at the hot-pressing temperature, are distributed along grain boundaries mainly in A30 (Fig. 1c) and in discrete pockets in A15 and A5; their amount decreases with decreasing SiC content [20].

Hot-pressed materials were cut into samples 8 mm × 8 mm × 1.5 mm, the surfaces were polished with successive diamond pastes up to 1μm and carefully washed. Oxidation tests were conducted in a kiln in air at 1400 °C for periods of 25, 50, 75, 100, 150 h. Some tests were also performed at 1100 and 1200 °C. The heating and cooling rates were 230 °C h^{-1} and 400 °C h^{-1}, respectively.

Before and after the tests, the samples were weighed with an analytical balance (± 0.02 mg). The reaction products were characterized using X-ray diffraction (XRD), scanning electron microscopy (SEM) and energy-dispersive microanalysis (EDM). The thickness of the reaction product layer was measured on scanning electron micrographs of sample cross-sections.

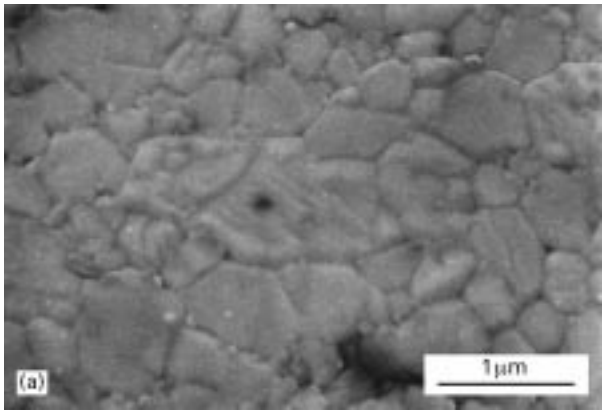

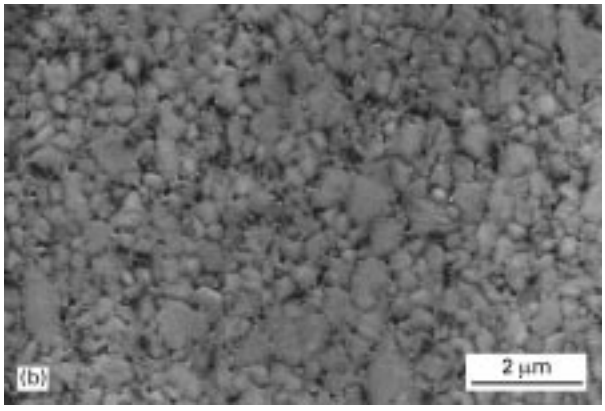

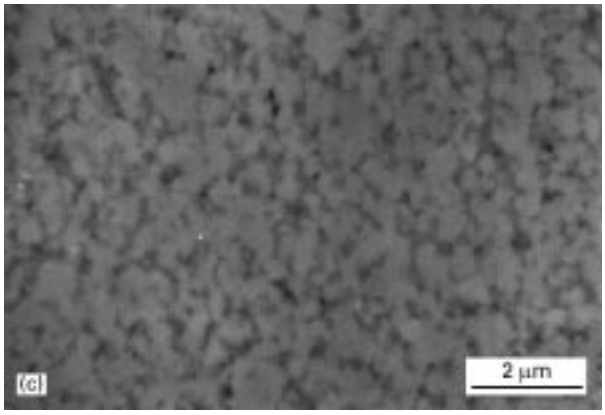

Figure 1a–c Surface morphology of the polished and thermally etched surface of samples: (a) A5, (b) A15 and (c) back-scattered electron image of the polished surface of sample A30.

3. Results

3.1. Reaction rates

Oxidation tests at 1100 °C did not result in weight change, and the very low values relative to long-term tests at 1200 °C were hardly detectable.

Table II gives the values of the weight gain per unit area, w, and oxide scale thickness, x, after the oxidation tests at 1400 °C. Process rate laws and the values of the rate constants (k_w and k_x obtained, respectively, from w and x data) are also reported. Figs. 2, 3 show the plots of w and x versus time. The observed data are not consistent with the expected increase in weight associated with the oxidation reaction of SiC to SiO_2. In fact, the most surprising feature is that sample A30, containing the highest amount of SiC particles, shows a better oxidation resistance than samples A5 and A15. The analysis of kinetics evinces the following peculiar features.

Sample A5: the results fit straight lines, indicating that the oxidation process follows a linear law, with $k_x \sim 1.2\,\mu m\,h^{-1}$ and $k_w \sim 8 \times 10^{-3}\,mg\,cm^{-2}h^{-1}$.

Sample A15: the definition of the process rate law is more complex than in the previous case; considering all the experimental data, a parabolic law fits the data better than a linear law, but this approach is not

TABLE II Values of the weight gains, w (relative to the sample surface area, s) and oxide scale thickness, x, after the oxidation tests. Process rate laws and rate constants k_w and k_x were calculated from the reported w and x data, respectively

		A_5		A_{15}		A_{30}	
T (°C)	t (h)	$\Delta w/s$ (mg cm^{-2})	x (μm)	$\Delta w/s$ (mg cm^{-2})	x (μm)	$\Delta w/s$ (mg cm^{-2})	x (μm)
1200	100	0.098		0.087		0.24	
1400	25	0.21 ± 0.06	33.5	0.45	29.3	0.31	11.4
1400	50	0.45 ± 0.05	58.8	0.97	56.5	0.39	14.9
1400	75	0.75 ± 0.05	90.1	1.48	87.7	0.53	19.1
1400	100	0.77 ± 0.06	99.2	1.51	92.0	0.72	21.5
1400	150	1.52 ± 0.06	196.2		112.0	0.95	28.6
		linear law		*linear law up to 75 h* $k_{w1} = 2\times10^{-2}$	$k_{x1} = 1.2$	*parabolic law*	
		$k_w = 8\times10^{-3}$ (mg cm^{-2}h^{-1})	$k_x = 1.2$ (μm h^{-1})	*after 75 h* $k_{w2} = 1.2\times10^{-3}$ (mg cm^{-2}h^{-1})	$k_{x2} = 0.33$ (μm h^{-1})	$k_w = 6\times10^{-3}$ (mg^{2}cm^{-4}h^{-1})	$k_x = 5.3$ (μm^{2}h^{-1})

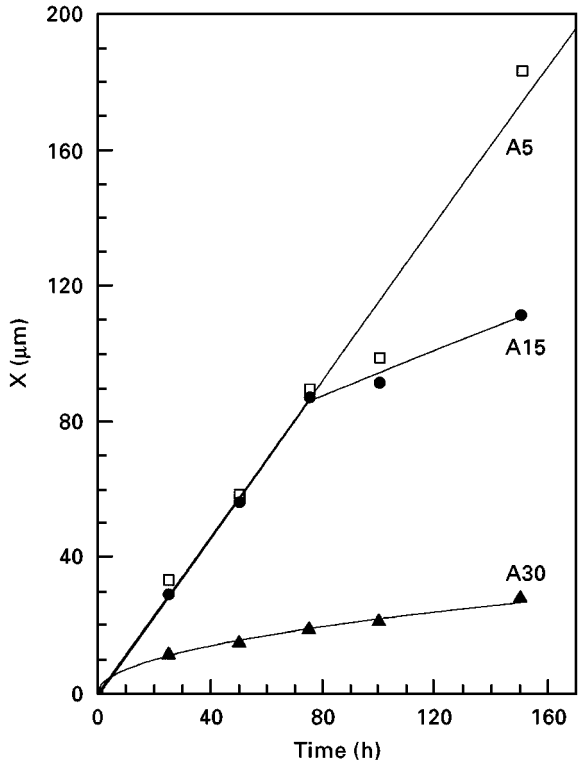

Figure 2 Plot of the reaction product thickness, x, as a function of the oxidation time at 1400 °C.

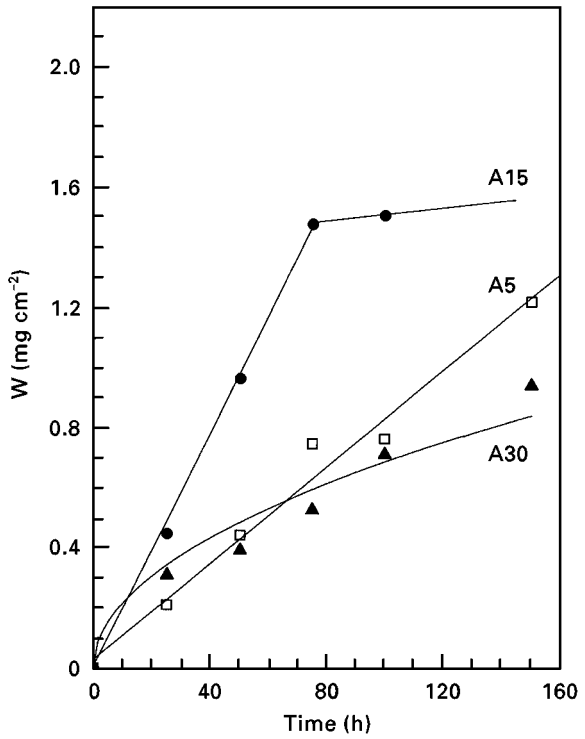

Figure 3 Plot of the weight gain per unit area, w, as a function of the oxidation time at 1400 °C.

satisfactory. It seems more reasonable to assume two stages: the first, up to 75 h exposure time, during which the process follows a linear law ($k_x \sim 1.2\,\mu m\,h^{-1}$ and $k_w \sim 2\times10^{-2}\,mg\,cm^{-2}\,h^{-1}$); and the second, for which the kinetics cannot be defined with certainty (under the hypothesis of a linear law, the process rates are about one quarter of those calculated for the first stage; actually a parabolic law is probable.)

Sample A30: this exhibits a parabolic oxidation behaviour, with the following rate constants: $k_x = \sim 5.3\,\mu m^2\,h^{-1}$ and $k_w = \sim 6\times10^{-3}\,mg^2cm^{-4}\,h^{-1}$.

Even if the absolute values of scale thickness differ little from those reported on alumina/silicon carbide composites with low amounts (< 20 vol %) of SiC, other features are different from those shown in the literature [25], particularly concerning (i) mass change, which in the present case is not directly related to the amount of SiC, and (ii) oxidation kinetics, previously observed to be always parabolic in similar materials [22, 23, 25]. In the present case, the occurrence of different kinetics with the variation of SiC amount indicates that different mechanisms govern the oxidation process of these nanocomposites, as discussed later.

The results confirm that the oxidation rate of SiC in the composites is higher than pure SiC: in fact, values

of 1–2 μm for pure SiC oxide layer thickness were measured after tests at 1375 °C for 72 h and parabolic oxidation rate constants three orders of magnitude higher in the composites have been previously reported [25].

3.2. Characterization of the reaction product

The hot-pressed nanocomposites are dark grey-black in colour, which is typical of samples hot pressed using a graphite die. After short oxidation tests, the surface of samples A5 and A15 becomes lighter and changes to a lighter grey colour with increasing exposure time. On the contrary, the grey–black colour of the original material is retained after all the oxidation tests in sample A30.

Typical features of the oxidized surface topography are shown in Figs 4a, b (A5), 5a–c (A15), and 6 (A30), for samples treated for 100 h at 1400 °C.

In samples A5 and A15, generally the morphology is not uniform: there are some large areas up to 50 μm (in A5) and up to 200 μm (in A15) of glassy phase holding escape pores and piles of elongated grains distributed in a fine-grained matrix. Beside oxygen, the only elements present in this matrix are aluminium and silicon, while the glassy bubbles contain traces of elements as potassium, calcium and sodium (deriving from the secondary phase of the hot-pressed nanocomposites); the elongated grains are crystalline mullite. On the oxidized surface of sample A15

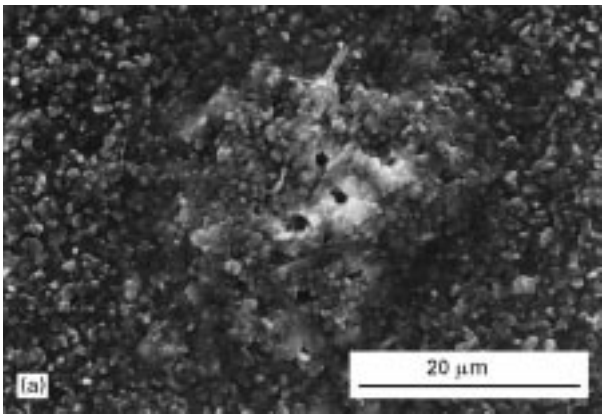

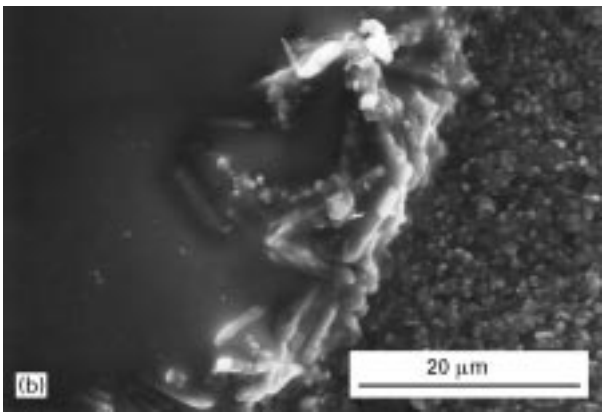

Figure 4a, b. Surface morphology of sample A5 oxidized for 100 h at 1400 °C: (a) general aspect, (b) an area of glassy phase with mullite grains.

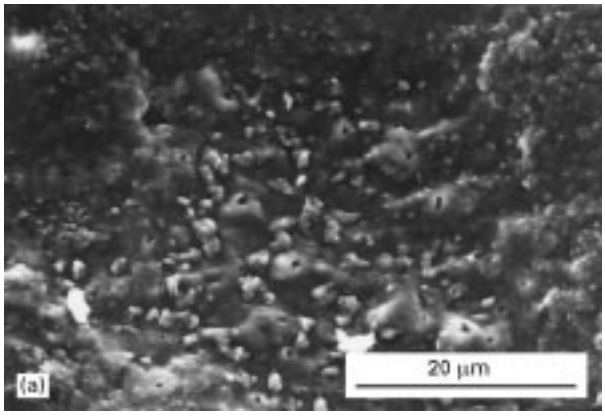

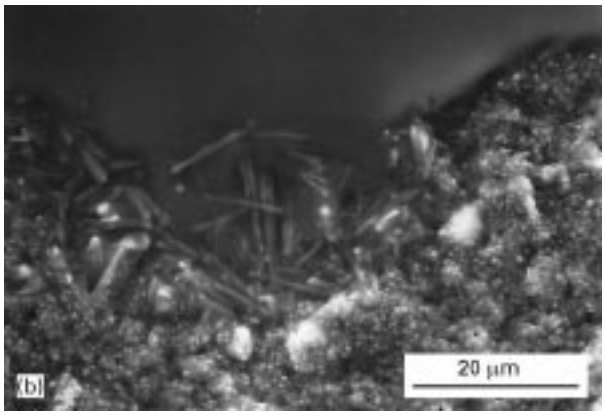

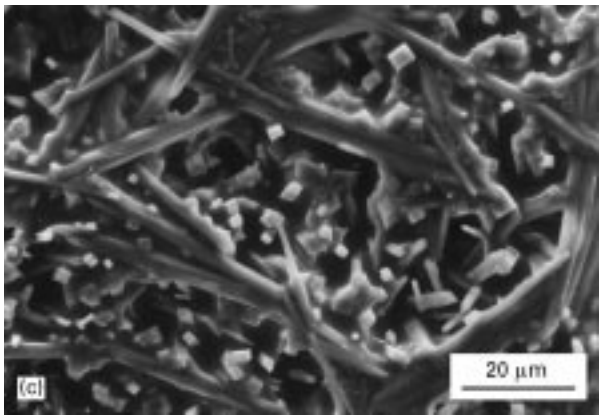

Figure 5a–c Surface morphology of sample A15 oxidized for 100 h at 1400 °C: (a) general aspect, (b) an area of glassy phase with elongated mullite grains; (c) oriented mullite grains.

(Fig. 5c), mullite grains have grown with a preferential orientation in the (0 0 1) and (0 0 2) crystallographic direction, as confirmed by X-ray analysis.

The surface morphology of sample A30 shows features different from those observed on A5 and A15: the reaction product is a continuous aluminosilicate glassy phase which contains a distribution of escape pores and of elongated mullite crystals. The observed features do not vary significantly with the oxidation time.

Cross-sections of the reaction products formed during oxidation reveal further details. In all the cases, there are no SiC particles in the reaction product, suggesting that SiC was oxidized completely. In sample A5 (Fig. 7a, b) the interface between oxide scale and unreacted composite is sharp and the reaction

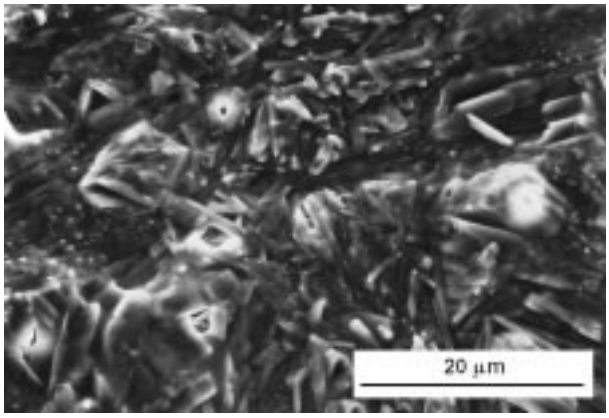

Figure 6 Surface morphology of sample A30 oxidized for 100 h at 1400 °C.

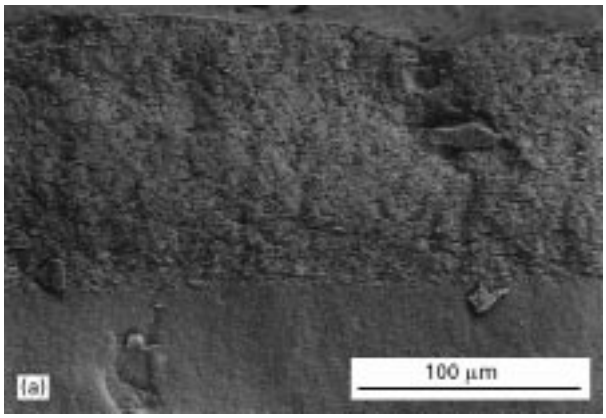

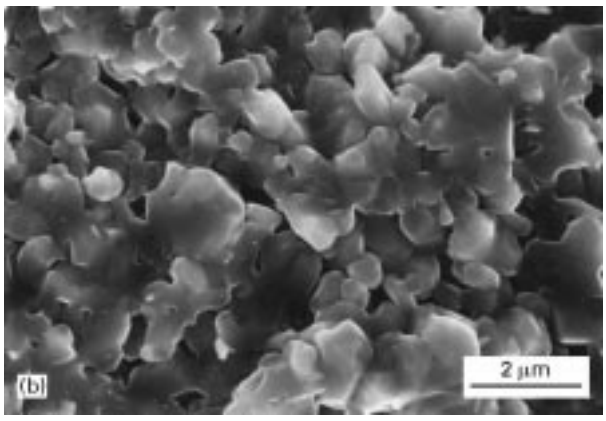

Figure 7a, b. Cross-section of sample A5 oxidized at 1400 °C: (a) back-scattered image of the reaction product layer showing a porous structure, (b) high magnification image of the oxidation product.

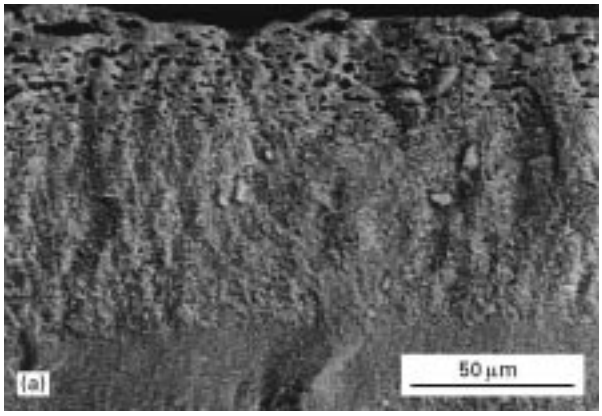

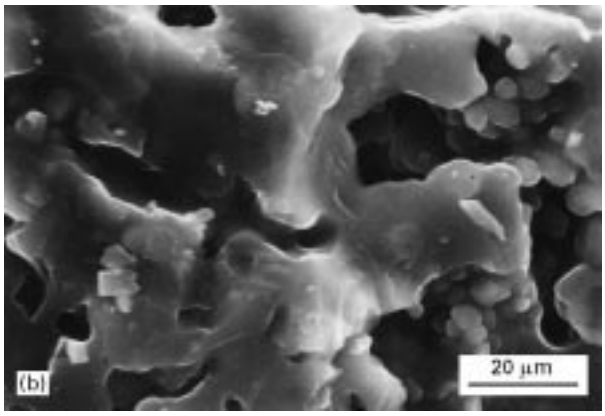

Figure 8a, b Cross-section of sample A15 oxidized at 1400 °C: (a) back-scattered image of the reaction product layer showing a graded structure, (b) high-magnification image of the upper part of the external layer in contact with the atmosphere.

product is porous and contains microcracks. This low density is assumed to be due to a combination of volume expansion during the formation of the product layer and possibly thermal expansion mismatch between the product and reactant during cooling. In fact, oxidation of SiC results in an expansion of ~100 % [25], and in alumina/silicon carbide composites non-protective scales were found to result from the formation of a rigid crystalline product, whose volume is at least 15 % greater than that of the bulk material [22]. In sample A15 (Fig. 8a, b) the oxide scale is composed of two layers of different thickness. The external one, relatively thinner, has pores and channels and is constituted by an aluminosilicate phase also containing traces of impurity cations. The inner layer, in contact with the unreacted bulk, has small-size pores and the only elements detected are aluminium, silicon and oxygen. Also in sample A30 (Fig. 9), the oxide scale, though very thin, is formed by two layers. The external one is an aluminosilicate phase containing impurities, mullite crystals and open and interconnected paths for the emission of the gaseous phase coming from the reaction of SiC to SiO_2. Between this scale and unreacted bulk there is a very thin highly porous layer, with a morphology similar to the oxide scale of A5.

X-ray diffraction analyses of the oxidized surfaces show alumina and mullite in samples A5 and A15: the alumina/mullite ratio is ~4 in A5 and ~0.7 in A15. Mullite and traces of trydimite (SiO_2) are the only crystalline phases constituting the reaction product of A30.

The observed compositions of oxidation products are in partial agreement with those expected on the basis of the Al_2O_3–SiO_2 phase diagram: under equilibrium conditions, the reaction product should contain alumina ad mullite for composites holding up to 24.4 wt % SiC particles (as in our A5 and A15 composites) and mullite and silica for higher percentages of SiC (as in composite A30, which contains 25.8 wt % SiC) [25]. However, beside these crystalline phases, an amorphous glassy phase has been observed in all the surface scales, although in different amounts and

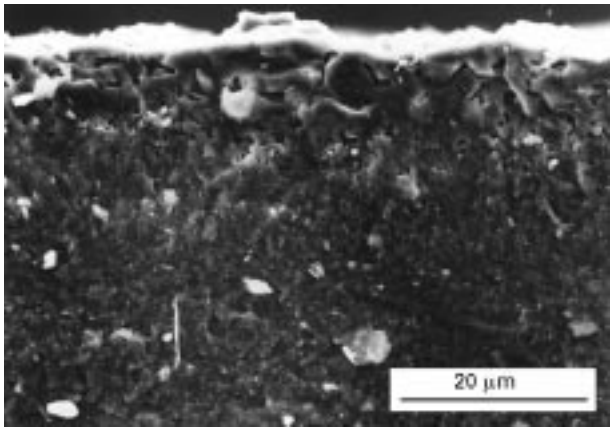

Figure 9 Cross-section of sample (A30) oxidized at 1400 °C showing: a thin layer in contact with the unreacted bulk containing micropores, and an external layer of glassy phase and mullite containing large pores and interconnected channels.

distribution, depending on sample composition. These results show that the reaction products are not in thermodynamic equilibrium, in agreement with previous analysis on alumina–SiC and mullite–SiC composites [25]. Moreover, the diffusion of impurities cations from bulk to reaction interface locally modifies composition and viscosity of the phases resulting from the reaction of silica with alumina, and contributes to the formation of glassy amorphous areas, where mullite crystals nucleate and grow.

4. Discussion

When an alumina/silicon carbide composite is exposed to an oxidizing environment, the SiC oxidizes to form SiO_2 with a weight gain. The reactions can be expressed as:

the oxidation reaction

$$SiC(s) + 3/2O_2(g) = SiO_2(s, l) + CO(g) \qquad (1)$$

and further reaction with alumina matrix to form mullite

$$2SiC(s) + 3Al_2O_3(s) + 3O_2(g) = 3Al_2O_3 \cdot 2SiO_2(s) + 2CO(g) \qquad (2)$$

These equations represent the overall reactions, irrespective of the form (ionic or molecular) in which oxygen is diffusing through the reaction product.

The reaction rates are influenced by the inward diffusion of oxygen, as well as by the outward diffusion of carbon monoxide, while it has been discounted that the reaction occurred by outward diffusion of aluminium or silicon [25, 26].

The overall oxidation process of these alumina–silicon carbide nanocomposites is complex, and is influenced not only by the amount of oxidizable phases, but also by the alumina content in the product layer and by the presence of impurities in the matrix; depending on the combination of these features, a protective or non-protective scale can result.

Sample A5 and A15: The linear kinetics with plots which go through the origin indicate that the scale is non-protective and that its growth is controlled by oxidation reaction of SiC particles at the interface between the oxidation product and unreacted bulk. As expected from phase diagrams, the reaction product contains alumina and mullite and no silica. It has been shown [22] that, with little or no unreacted silica, the product layer is rigid and unable to relieve stresses rapidly enough to prevent bulging. Therefore, the reaction product characteristics would be influenced by the volume change associated with oxidation, as confirmed by the morphological aspects described above. When, as in these samples, the reaction product contains liquid phase in small amounts and distributed in discrete, separated areas, the volume expansion is not accommodated by squeezing out of the liquid phase. Even if the scale does not spall off, the coating may be disrupted by high internal stresses, thereby allowing oxygen to diffuse rapidly to the interface. The disrupted coating also permits easy escape of gaseous reaction products.

In the absence of any interaction between silica produced by oxidation of SiC, alumina matrix and impurities, the thickness and weight gain of the oxidation product should be proportional to the amount of oxidizable phases. Actually we have observed that the weight gain rate for sample A15 (up to 75 h of oxidation) is higher by a factor of 2.5 than the value measured for sample A5, while, on the basis of the amount of SiC, the expected value should be 3. On the contrary, the oxide layer growth rate is about the same in the two materials. This could be related to (i) the most porous morphology of the oxidation product in A5, due to the above mentioned mechanical considerations of the thermal expansions of the present phases, (ii) the relative amount of alumina inside the oxide scale. Alumina, in fact, has been observed to increase the diffusion of oxygen to the interface: oxidation rates for pure SiC are enhanced by a factor of 10–20 in comparison with those for SiC contained in either alumina or mullite matrices [22]. In sample A15, after 75 h exposure time, the oxidation rate (under the hypothesis of a second linear stage) decreases at about one-quarter of the values observed in the first stage. Actually, we have insufficient data to determine whether the first linear stage is followed by a linear or parabolic stage. The two-stage regime can be explained on the basis of the layered oxidation scale, where the external layer has a protective-like morphology (Fig. 8a, b), contains mullite and aluminosilicate liquid, and is four times thinner than the non-protective layer in contact with the unreacted bulk.

Moreover the presence in the oxide product of alumina together with an amount of silica lower than the stoichiometric one necessary to form mullite can result in the creation of either a metastable eutectic or immiscible non-equilibrium aluminosilicate liquid, as already shown [22]. This influences oxygen permeability through the oxidation product which has been estimated faster through aluminosilicate or mullite than that through alumina [25]. The presence of impurities, which locally concentrate in discrete areas,

can produce additional decrease of the silica eutectic temperature and a consequent increase of oxygen diffusion rate through the oxidation layer, as also previously reported [22]. These elements have contributed to form the observed amorphous phase regions or bubbles of liquid aluminosilicate phase.

Sample A30: Protective scales exhibiting diffusion-controlled oxidation behaviour occurred; here the reaction layer contains sufficient silica to place the scale composition in the mullite–rich side of the mullite–alumina two-phase field of the alumina–silica phase diagram. As expected, in fact, beside mullite, crystalline trydimite is also present, although in trace amounts. The viscous nature of the coating, which also contains some impurities, dissipates stresses associated with volume expansion, avoids coating disruption and buckling and ensures a protective nature of the reaction scale. The reaction rates are supposed to be controlled by the inward diffusion of oxygen, considering that the outward escape of carbon monoxide is favoured by the interconnected channels and pores present in the surface oxide scale.

It is important to point out that, under the same experimental conditions, the product layer thickness in sample A30 is one-third to one-fifth of that formed on sample A5, in spite of the amount of oxidizable phase which in A30 is six times higher. On the other hand, in these two samples (A5 and A30), the weight gains are similar after exposure times up to 100 h, confirming the protective action of the reaction product layer in A30.

The evolution of the oxidation process in Al_2O_3–SiC composites can be outlined as follows:

(a) reaction of SiC particles on the sample surface with oxygen to form a thin surface layer of silica which has a very low permeability to oxygen;

(b) while the oxidation of SiC particles is continuing, the so-formed silica reacts with alumina producing mullite or aluminosilicate liquid, through which oxygen permeabilities are much higher. These reactions are favoured by diffusion of alkaline cations from the bulk, which lower the eutectic liquidus temperature. Depending on the actual ratio alumina/silica, two different structures can arise: (i) layers constituted of alumina and mullite, containing a high amount of small pores and microcracks; (ii) compact layers constituted by mullite and silica and possibly glassy aluminosilicates, containing large pores and interconnected channels;

(c) the oxidation product grows with a two-layered structure: a non-protective porous and buckled layer in contact with the unreacted material, which acts as a fast path for oxygen to the reaction interface, and an external protective layer whose composition and morphology controls the diffusion of oxygen and the escape of carbon monoxide.

The correspondence of these phenomena with our experimental results was examined.

In sample A5, the external layer is absent and silica or glassy aluminosilicate phase or mullite are distributed only in local areas. The oxidation product is non-protective, the rate-controlling step being the reaction at the interface. In sample A30, owing to the higher amount of uniformly distributed silica formed in the early stage, the external protective layer of aluminosilicate phase and mullite covers the whole surface. The kinetics is parabolic and the rate-governing mechanism can be either the diffusion of oxygen to the reaction interface or the outward diffusion of carbon monoxide. The observed morphology suggests the former mechanism, as the interconnected channels and pores present in this layer are an easy path for gaseous molecular carbon monoxide. In sample A15 the initial stage (up to 75 h) is characterized by a process similar to that described in sample A5 (reaction at the interface is rate controlling); subsequently a condition is reached which favours the formation of a protective external layer similar to sample A30.

The results stress that when designing alumina-based composites with oxidizable SiC as reinforcing phase, it is important that the amount of silica produced by reaction of SiC is sufficient to convert all alumina in the oxidation scale to mullite. Too little silica will result in the formation of a rigid scale which will delaminate and provide non-protective qualities, as previously observed in Al_2O_3–$MoSi_2$ composites [22]. The formation of mullite or mullite plus silica will be protective but could spall off during thermal cycling due to thermal mismatch between the coating and the substrate.

In agreement with previous assessment [22], alumina should not be considered a good host for silicon-based reinforcing phases in the production of ceramics for high-temperature applications under oxidizing environments.

5. Conclusion

The oxidation behaviour of dense hot-pressed Al_2O_3–SiC nanocomposites, containing 5, 15 or 30 vol % ultrafine SiC particles, has been tested at 1400 °C for exposure times up to 150 h. Weight gains and thickness of the oxide scales have been measured, and the structure and composition of the reaction products examined: mullite and alumina are the crystalline phases constituting the reaction product in A5 and A15, while mullite and traces of silica have been found on the surface of A30.

The experimental data confirm that these composites have a lower thermal stability than monolithic SiC. Kinetics (linear or parabolic) and oxidation rates depend on the amount of oxidizable phase in the composite, on the presence of alumina in the oxide scale and on the presence of impurities. All these elements determine the protective or non-protective nature of the reaction product.

Linear kinetics have been observed in composites containing 5 and 15 vol % SiC (in this latter case only up to 75 h exposure time). The reaction product thickness is the same in the two samples, while the weight gain is higher in the composites containing 15 vol % SiC. The oxidation reaction of SiC particles is supposed to govern the process and oxide scale grows porous and non-protective, owing to volume changes or thermal mismatches between oxidation products and matrix.

The kinetics are parabolic in composites containing 30 vol % SiC as the reaction product contains sufficient silica to convert all the alumina to mullite; the resulting coating is protective in that its viscous nature is able to dissipate stresses arising from volume expansions. The total weight gain and reaction product thickness are lower than in samples containing 5 and 15 vol % SiC. The process is supposed to be controlled by the diffusion of oxygen through the oxide scale.

References

1. M. STERNITZKE, *J. Eur. Ceram Soc.* **17** (1997) 1061.
2. K. NIIHARA, *J. Ceram. Soc. Jpn* (Int. Ed.) **99** (1991) 945.
3. T. OHJI, T. HIRANO, N. NAKAHIRA and K. NIIHARA, *J. Am. Ceram. Soc.* **79** (1996) 33.
4. L. TIMMS, B. LE RAZER, D. H. PEARCE, A. JICKELLS and C. B. PONTON, in "Fourth Euro Ceramics", Vol 4, edited by A. Bellosi (Faenza Editrice, 1995) Faenza, pp. 37–44.
5. L. C. STEARNS, J. ZHAO and M. P. HARMER, *J. Eur. Ceram. Soc.* **10** (1992) 437.
6. J. ZHAO, L. C. STEARNS, M. P. HARMER, H. M. CHAN, G. A. MILLER and R. E. COOK, *J. Am. Ceram. Soc.* **76** (1993) 503.
7. H. WOHLFROMM, in Ceramic Transaction Vol. 51, "Ceramic Processing Science and Technology", edited by H. Hausner, G. L. Messing, S. Horano (The American Ceramic Society, 1995) Westerville, Ohio, pp. 658–63.
8. C. E. BORSA and R. J. BROOK, *ibid*., pp. 653–58.
9. M. ALSAN, C. DORR, R. NASS and H. SCHMIDT, *ibid*., pp. 665–9.
10. A. M. THOMPSON J. FANG, H. M. CHAN and M. P. HARMER, *ibid*., pp. 671–9.
11. A. PICIACCHIO, S.-H. LEE and G. MESSING, *J. Am. Ceram. Soc.* **77** (1994) 2157.
12. Y. XU, A. ZANGVIL and A. KERBER, *J. Eur. Ceram. Soc.* **17** (1997) 921.
13. Y.-F. ZHANG, Z.-Y. DENG, J.-L. SHI , Y.-Q. MAO and J.-K. GUO, *J. Mater. Sci. Lett.* **15** (1996) 1927.
14. C. C. ANYA and S. G. ROBERTS, *J. Eur. Ceram. Soc.* **17** (1997) 565.
15. C. E. BORSA, N. M. R. JONES, R. J. BROOK and R. I. TODD, *ibid.* **17** (1997) 865.
16. D. O' SULLIVAN, M. POORTEMAN, B. THIERRY, A. LERICHE, P. DESCAMPS and F. CAMBIER, *Silica Industriels* **11-12** (1996) 235.
17. Y. SAKKA, D. D. BILDINGER and I. A. AKSAY, *J. Am. Ceram. Soc.* **78** (1995) 479.
18. I. A. CHOU, H. M. CHAN and M. P. HARMER, *ibid.* **79** (1996) 2403.
19. Z.-Y DENG, Y.-F. ZHANG, J.-L. SHI and J.-K. GUO, *J. Eur. Ceram. Soc.* **16** (1996) 1337.
20. D. SCITI, D. DALLE FABBRICHE and A. BELLOSI, in "Key Engineering Materials Vols 132–136", Euro Ceramics V, Part 3, J. Baxter, L. Cot, R. Fordham, V. Gabis, Y. Hellot, M. Lefebvre, H. Ledoussal, A. Le Sech, R. Naslain, A. Sevagen (Eds) (1997) Trans Tech. Publications, Vetikov-Zue Rich, Switzerland, pp. 2001–4.
21. R. E. TRESSLER, in "Corrosion of Advanced Ceramics", edited by G. Nickel, NATO ASI Series, (Kluwer Academic, 1994) pp. 3–22.
22. M. P. BOROM, M. K. BRUN and L. E. SZALA, *Ceram. Eng. Sci. Proc.* **8**, The American Ceramic Society, Westerville, Ohio (1987) 654.
23. K. LUTHRA, *ibid.* **8** (1987) 649.
24. R. A. MARRA and D. J. BRAY, *ibid.* **7** (1986) 945.
25. K. L. LUTHRA and H. D. PARK, *J. Am. Ceram. Soc.* **73** (1990) 1014.
26. T. KENNEDY, J. BROWN, J. DOYLE and S. HAMPHIRE, in "Key Engineering Materials". Vol. 113, "Corrosion of Advanced Ceramics", R. J. Fordham, D. J. Baxter, T. Graziani (Eds.) (Trans Tech, Switzerland, 1996) pp. 65–70.

Received 17 October 1997
and accepted 15 May 1998